Kinetics of NO and NO_2 Evolution from Illuminated Frozen Nitrate Solutions

C. S. Boxe,[†] A. J. Colussi,*[,†] M. R. Hoffmann,[†] I. M. Perez,[‡] J. G. Murphy,[‡] and R. C. Cohen[‡]

W. M. Keck Laboratories, California Institute of Technology, Pasadena, California 91125, and Department of Chemistry and Department of Earth and Planetary Sciences, University of California, Berkeley, California 94720

Received: September 6, 2005; In Final Form: January 24, 2006

The release of NO and NO_2 from frozen aqueous $NaNO_3$ irradiated at 313 nm was studied using time-resolved spectroscopic techniques. The kinetic behavior of NO and NO_2 signals during on-and-off illumination cycles confirms that NO_2 is a primary photoproduct evolving from the outermost ice layers and reveals that NO is a secondary species generated deeper in the ice, whence it eventually emerges due to its inertness and larger diffusivity. NO is shown to be more weakly held than NO_2 by ice in thermal desorption experiments on preirradiated samples. The partial control of gaseous emissions by mass transfer, and hence by the morphology and metamorphisms of polycrystalline ice, is established by (1) the nonmonotonic temperature dependence of NO and NO_2 signals upon stepwise warming under continuous illumination, (2) the fact that the NO, NO_2 or NO_x ($NO_x \equiv NO + NO_2$) amounts released in bright thermograms performed under various heating ramps fail to scale with photon dose, due to irreversible losses in the adsorbed state. Because present NO/NO_2 ratios are up to 10-fold smaller than those determined over sunlit snowpacks, we infer that the immediate precursors to NO mostly absorb at $\lambda > \lambda_{max}$ (NO_3^-) $\sim$ 302 nm.

Introduction

The finding that elevated NO_x ($NO_x \equiv NO + NO_2$) levels develop in and above snowpacks during early spring[1,2] has revived interest in the nitrogen cycle over polar regions. NO_x emissions originate from the solar photolysis of embedded nitrate, a ubiquitous contaminant of snow and ice absorbing above 300 nm.[3] The interpretation of NO_x fluxes from snow and ice measured at various geographical locations corresponding to different sets of nitrate concentrations, solar irradiances/zenith angles, and ambient temperatures, remains a challenge.

Thus, NO_x fluxes, R_{NO_x}, into the atmospheric boundary layer over the South Pole, $R_{NO_x} \sim 3 \times 10^8$ molecules cm^{-2} s^{-1},[4] exceed those at other Antarctic or Arctic sites during the summer solstice, even after factoring out differences in nitrate concentrations and solar irradiances.[5] If R_{NO_x}'s were exclusively determined by nitrate photolysis, the Summit (Greenland) site should have recorded the highest values, at variance with observations. Both NO and NO_2 production rates (in molecules cm^{-3} s^{-1}) in the snowpack display significant and reproducible daily variations.[2,6] NO_x mixing ratios, which are proportional to NO_x production rates (or fluxes), are consistently larger inside the snowpack than in ambient air during the day, pointing to a photochemical process driven by sunlight. Field experiments performed at noon over artificial snow made by freezing 100 μM $NaNO_3$ solutions yield $\gamma = R_{NO}/R_{NO_2} \sim 0.1$, a value that increases about 10-fold upon addition of free radical scavengers.[7] Irradiation of Antarctic snow at $\lambda \geq$ 295, 320, 345 and 385 nm shows that NO_x production ceases above 345 nm, confirming nitrate as the primal chromophore, and that γ is an increasing function of cutoff wavelength.[3] The abnormally large NO_x fluxes detected at the South Pole have been tentatively ascribed to the prevailing lower temperatures,[8] although NO_x production rates in snow chamber experiments seem to be independent of temperature between −30 and −20 °C,[3] or positively correlated with temperature in laboratory experiments on nitrate photolysis in ice.[9,10] The reasons for the larger HONO and $HONO_2$ vertical fluxes observed at the South Pole relative to other sites have not yet been identified.[6,8,11−13] A recent study suggested that cation speciation underlies the significant differences between inland and coastal Arctic regions for the release/uptake of these acids.[14,15]

It is apparent that field measurements are affected by an open set of physical and chemical factors that operate through still unraveled mechanisms. Laboratory studies on snow chemistry and photochemistry under controlled conditions may prove essential for advancing our understanding of these phenomena. We,[10,15−17] and others,[7,9] have performed quantitative studies on the photochemistry of nitrate in its frozen aqueous solutions. The monotonic temperature dependence of NO_2, NO_2^- and NO photoproduction rates above and below the normal freezing point provide strong evidence that a similar mechanism operates in fluid and frozen nitrate solutions down to subeutectic temperatures.[10,16,17] We also showed that the amounts of NO_2 photodesorbed during temperature-programmed nitrate photolysis scale less than linearly with the duration of the experiments or with nitrate concentration, and that NO_2 emission rates display abrupt transitions likely related to structural relaxations of the ice matrix.[15]

Here we report time-resolved NO(g) and NO_2(g) fluxes from frozen nitrate solutions irradiated at $\lambda = 313$ nm above −30 °C. The present study focuses on the differential responses of R_{NO} and R_{NO_2} to the onset and interruption of illumination, and to temperature variations under isothermal or temperature-programmed regimes.

Experimental Section

The photoreactor used in these experiments has been described in detail previously.[15,16] About 6 mL of aqueous $NaNO_3$

* Corresponding author. E-mail: ajcoluss@caltech.edu.
[†] California Institute of Technology.
[‡] University of California.

10.1021/jp055037q CCC: $33.50
Published on Web 02/23/2006

(EM Science) solutions (pH ≤ 6) are sprayed onto a cooled finger (CF, $a = 304$ cm^2) where they instantly freeze into porous, polycrystalline ice layers. The temperature of the ice layers is controlled by a programmable cryogenic unit (Thermo Neslab ULT-80) via coolant circulation through the CF. The ice-covered CF is enclosed within a fused silica sheath (QS) for illumination with the $\lambda = 313 \pm 20$ nm radiation emitted by four Hg Pen-Ray UV lamps (UVP, model 90−0001−04), which overlaps the $\lambda_{max}(NO_3^-) = 302$ nm absorption band of nitrate. The overall irradiance incident on the ice layers: $I_i = 3.0 \times 10^{15}$ photons cm^2 s^{-1}, is determined using potassium ferrioxalate as a chemical actinometer.[18] The gaseous NO and NO_2 photoproducts released into the volume delimited by the CF and the QS are continuously flushed into the detection zone by means of zero-air carrier gas ($F_C = 2.5$ L min^{-1} at 1 atm, 293 K) within 11 s.

NO(g) is detected via NO + $O_3 \rightarrow NO_2$* chemiluminescence (Thermo Electron Corporation, Model 42C-TL NO−NO_2−NO_x Analyzer).[19,20] NO_2* emits a broad continuum from 500 to 2800 nm ($\lambda_{max} \sim 1300$ nm),[21] which is detected with a red-sensitive (500−900 nm) photomultiplier tube. NO_2(g) is detected by laser-induced fluorescence. A pulsed dye laser is used to pump on and off a pair of overlapping rotational lines of the $A^2B_2 \leftarrow$ (000) X^2A_1 NO_2 vibronic band at 585.26 nm. Fluorescence is collected by a time-gated PMT detector in the range 750−1100 nm.[22] Both detection systems were calibrated with certified standard mixtures, have linear dynamic ranges exceeding 10 ppbv, i.e., much larger than the mixing ratios detected in present experiments, and response times shorter than 2 s. The time resolution of this setup is, therefore, largely determined by gas transit times from the photolysis zone to the detectors. All the results reported below represent the average of at least three reproducible experiments.

Results and Discussion

The photolysis of aqueous nitrate ($\epsilon_{max} = 7.5$ M^{-1} cm^{-1} at 302 nm) at $\lambda > 300$ nm, pH < 6 in fluid or frozen media proceeds via reactions (1) (∼90%) and (2) (∼10%):[9,10,23−29]

$$NO_3^- + H^+ \xrightarrow{h\nu} NO_2 + {}^\bullet OH \quad (1)$$

$$NO_3^- \xrightarrow{h\nu} NO_2^- + O(^3P) \quad (2)$$

The photolysis of both nitrite[30−34] and NO_2(g)[35,36] yield NO:

$$NO_2^- + H^+ \xrightarrow{h\nu} NO + {}^\bullet OH \quad (3)$$

$$NO_2 \xrightarrow{h\nu} NO + O(^3P) \quad (4)$$

NO_2(g) increasingly absorbs at wavelengths longer than 313 nm, decomposing with high quantum yield: $\phi_4 \sim 1$, at $\lambda \leq 395$ nm.[35] The conjugated acid HONO ($pK_a = 2.8$)[30] will efficiently photolyze into (NO + •OH) in the gas phase.[35] Note that reaction 5 ($k_5 \sim 2 \times 10^{10}$ M^{-1} s^{-1}):[31]

$$NO_2^- + {}^\bullet OH \rightarrow NO_2 + OH^- \quad (5)$$

rapidly converts NO_2^- into NO_2, unless •OH is efficiently scavenged by other species.[17]

Thus, NO_2 is a primary photoproduct of nitrate photodecomposition, reaction 1, but can be also produced in secondary reactions, such as reaction 5. The extent of NO_2 photolytic losses, reaction 4, is expected to increase with residence time.

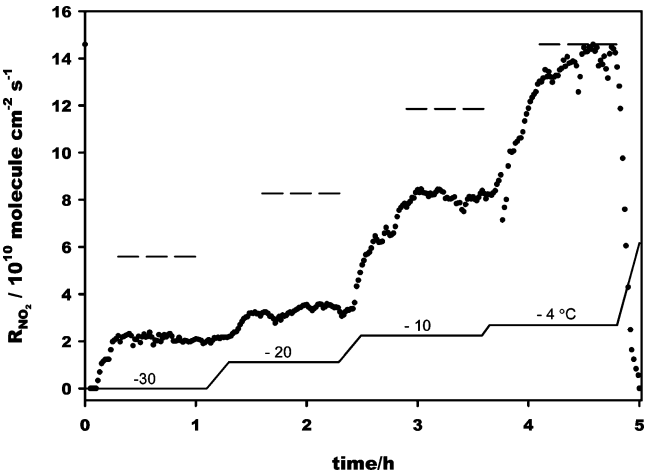

Figure 1. NO_2 emission rates, R_{NO_2}, from a continuously illuminated (at 313 ± 20 nm) 50 mM aqueous $NaNO_3$ solution frozen at −30 °C, and subsequently warmed along the temperature program indicated by the solid line at the bottom of the plot. The dashed segments correspond to estimated rates of photochemical NO_2 production from the quantum yields of •OH formation in reaction 1, ϕ_1, reported in ref 8.

NO and NO_2 residence times in polycrystalline ice are anticipated to be different on account of their relative molecular sizes and polarities. NO is a secondary species produced via reactions 3 and 4. Many species can act as sinks for the reactive •OH radicals. Their presence in natural snow and ice will critically perturb the delineated photochemistry, which strictly applies to frozen nitrate solutions.[7]

Under constant carrier gas flow rates, F_C, the NO_2 concentrations detected in the gas phase are directly proportional to release rates, r_{NO_2}, from the irradiated solid:

$$r_{NO_2} = J_{NO_3^-}\frac{\varphi_1}{\varphi_1 + \varphi_2} - \partial[NO_2]_S/\partial t - C - D = [NO_2]F_C \quad (6)$$

Thus, r_{NO_2} represents the balance between rates of photochemical production, $J_{NO_3^-}\varphi_1/(\varphi_1 + \varphi_2)$, accumulation in the solid, $\partial[NO_2]_S/\partial t$, and chemical, C, or photochemical destruction, D. Because $F_C = 41.7$ cm^3 s^{-1}, the detection of 1 pptv NO_x in the gas phase (1 part in 10^{12} per volume = 2.5×10^7 molecule cm^{-3} at 1 atm, 293 K) in this setup is equivalent to the release of $r = 1.0 \times 10^9$ molecules s^{-1} or, in terms of fluxes, of $R = 3.4 \times 10^6$ molecules cm^{-2} s^{-1} from the illuminated area (see Experimental Section). From the absorbance of ∼250 μm thick frozen 50 mM nitrate layers: $A = 7.5$ M^{-1} cm^{-1} × 5 × 10^{-2} M × 0.025 cm = 9.4×10^{-3}, the incident photon flux: $I_i = 3.0 \times 10^{15}$ photons cm^2 s^{-1}, and the quantum yields of •OH production in reaction 1: $\phi_1(^\bullet OH) = 36.6 \exp(-2400/T)$,[8] we estimate primary NO_2 production fluxes: 3.0×10^{15} photons cm^2 s^{-1} × 9.4×10^{-3} × $\phi_1(^\bullet OH) = 5.6$, 7.1, 11.6 and 14.2 × 10^{10} molecule cm^{-2} s^{-1}, at −30, −20, −10 and −4 °C, respectively. These estimated NO_2 *production* fluxes are shown in Figure 1 as dashed lines, along with actual NO_2(g) *emission* fluxes, R_{NO_2}, measured over steadily illuminated 50 mM $NaNO_3$ frozen layers. We do not attach much importance to the absolute agreement between both sets of data because the estimated fraction of incident light absorbed by the nitrate contained in our ice layers does not take into account light scattering, layer nonuniformity or the spectral mismatch between the actinometer and nitrate absorption spectra. Effective emission fluxes, R_{NO_2}, are expected, in principle, to be smaller than primary NO_2 production fluxes due to potential NO_2 losses prior to desorption.

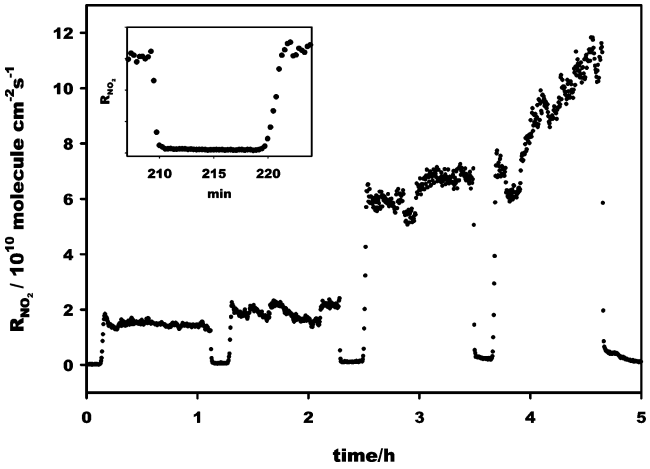

Figure 2. NO_2 emission rates, R_{NO_2}, from a frozen 50 mM aqueous $NaNO_3$ solution illuminated during the isothermal stages, at −30, −20, −10 and −4 °C, of the temperature program shown in Figure 1. The inset zooms in the transients following the cessation of illumination at the end of the −10 °C isothermal stage, and at the onset of illumination early in the −4 °C stage.

The increasingly larger NO_2 deficits observed at lower temperatures confirm that only a fraction of photogenerated NO_2 is released from ice. In contrast with the circumstantial agreement between absolute rate values, the observed dependence of R_{NO_2} on temperature represents a real effect because it involves relative rates obtained in a single experiment on the same ice sample.

In the experiments of Figure 1, the temperature of the CF, initially at −30 °C, was programmed to step up to −20, −10 and −4 °C at 0.7 °C min^{-1} after successive ∼ 1 h intervals. R_{NO_2} closely tracks temperature upon warming from −30 to −20 °C but slowly approaches a stationary value long after the system has reached −10 °C, an effect that becomes more pronounced at −4 °C. The slower, and nonmonotonic, response of R_{NO_2} to thermal perturbations at higher temperatures cannot be associated with an elementary photochemical process, but with desorption from an increasingly accessible pool of preformed NO_2. Figure 2 displays the result of a related experiment in which irradiation is interrupted during warming periods. In this case, NO_2 signals exponentially rise (decay) to steady-state values with characteristic times $\tau \sim 20$ s, following the onset (cessation) of illumination at lower temperatures, although they still fail to reach steady state even after 1 h at −4 °C. The observed τ's are longer than the response of the detection system and, therefore, represent a genuine effect. These experiments (Figures 1 and 2) confirm that R_{NO_2} does not accelerate gradually with T but markedly increases between −20 and −10 °C. Furthermore, the dissimilar responses to temperature jumps observed in Figure 1 vs Figure 2 starkly exposes the fact that photochemical and thermal effects are not separable in these systems. This phenomenon must be ascribed to the plasticity of an ice matrix whose microstructure, as experienced by NO_x species, is determined not only by temperature but also by external perturbations, such as ongoing photochemistry. A log R_{NO_2} vs 1000/T plot, based on the steady state R_{NO_2} values of Figures 1 and 2, is shown in Figure 3. By forcing a linear regression through these data, we obtain an apparent activation energy: $E_{NO_2} = (38.3 \pm 6.1)$ kJ mol^{-1}, which is compatible with the value ($E = 41.8$ kJ mol^{-1}) we had reported before for this process.[10] An Arrhenius temperature dependence for R_{NO_2} is an acceptable, i.e., within the given error limits, working

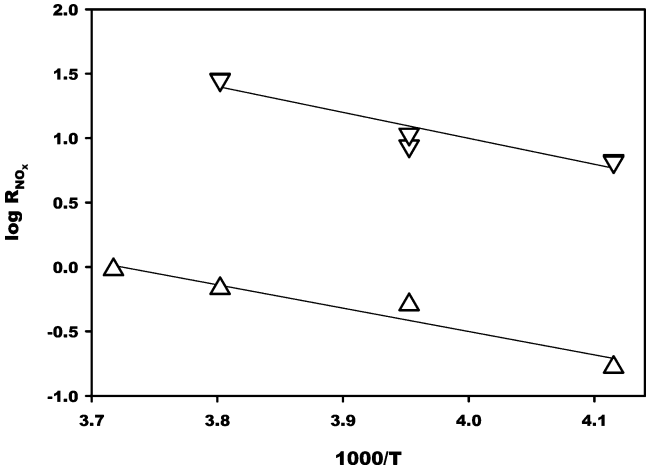

Figure 3. Arrhenius plots of R_{NO_x} rates. ▽: R_{NO_2}'s from Figures 1 and 2. △: R_{NO}'s from Figure 5.

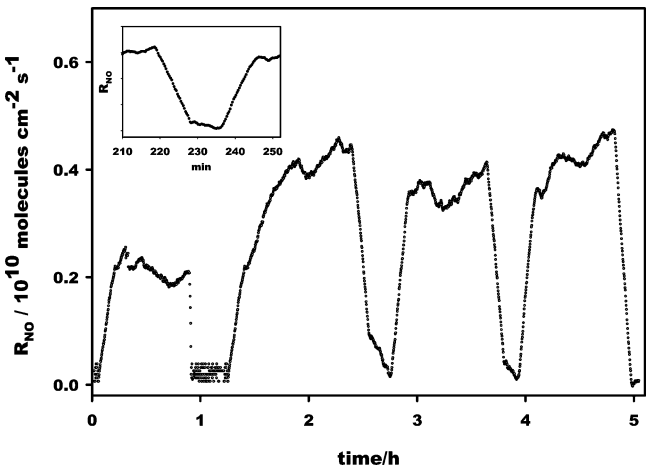

Figure 4. NO emission rates, R_{NO}, from a frozen 50 mM aqueous $NaNO_3$ solution illuminated during the isothermal stages, at −30, −20, −10 and −4 °C, of the temperature program shown in Figure 1. The inset zooms in the transients following the cessation of illumination at the end of the −10 °C isothermal stage, and at the onset of illumination early in the −4 °C stage.

assumption in these experiments that may, however, break down for other ices.

Nitric oxide is released quite differently in these experiments (Figures 4 and 5). Notice that the ratio of instantaneous rates: $\gamma = R_{NO}/R_{NO_2}$, varies between 0.1 and 0.043 (cf. Figures 1 and 5), depending on temperature. These values are about an order of magnitude smaller than the γ values measured in the field. The apparent discrepancy is likely due to the fact that both NO_2^- and NO_2, the immediate precursors of NO, increasingly absorb at wavelengths longer than 313 nm and, therefore, will undergo more extensive photolysis under sunlight. The corollary is that γ may also depend on factors affecting the solar spectrum such as zenith angle, altitude, latitude, season and time of day.[36] The responses of NO fluxes into the gas phase to the onset of illumination and darkness are qualitatively and quantitatively different than in the case of NO_2 (see the inset to Figure 4). R_{NO} increases and decreases linearly, rather than exponentially, as a function of time, with characteristic times $\tau \sim 300$ s vs ∼20 s for R_{NO_2}. In the case of NO, τ is defined as $\tau = {}^1/_2\,(t_{NO=O} - t_{NO=NO_0})$. This behavior rules out NO as a primary photochemical species. Furthermore, a linear R_{NO} vs time kinetics excludes desorption of a single monolayer of noninteracting NO molecules but may be rationalized in terms of NO emerging from increasingly populated deeper layers. The

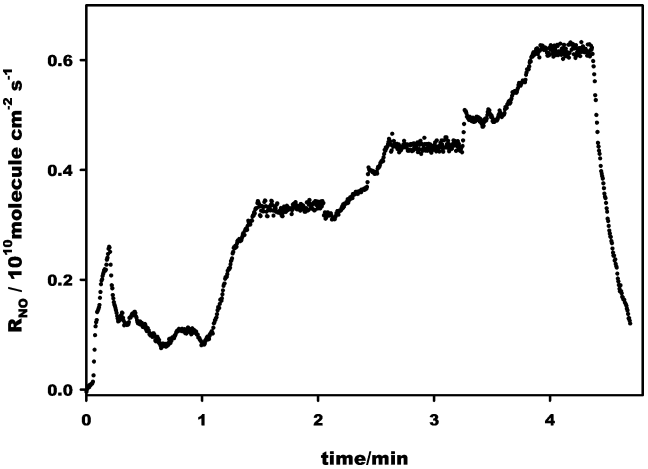

Figure 5. NO emission rates, R_{NO}, from a continuously illuminated 50 mM aqueous $NaNO_3$ solution frozen at −30 °C, and subsequently warmed along the temperature program shown in Figure 1.

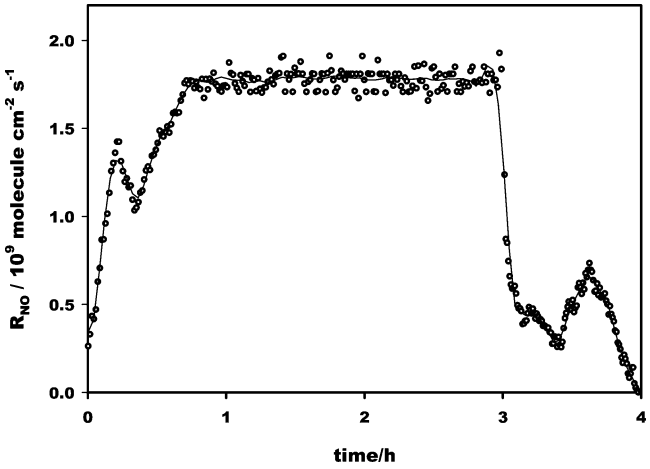

Figure 6. NO emission rates, R_{NO}, from a 50 mM aqueous $NaNO_3$ solution illuminated at −30 °C for 3 h, and then warmed at 0.5 °C min^{-1} in the dark for 1 h.

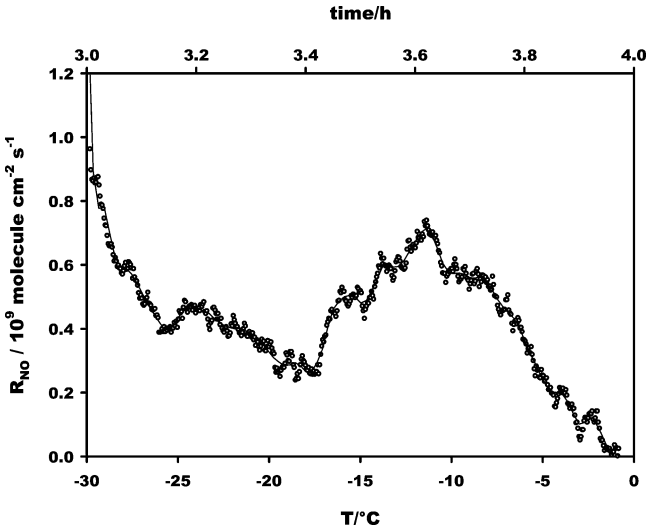

Figure 7. NO emission rates, R_{NO}, during a 0.5 °C min^{-1} dark thermogram performed on a frozen 50 mM aqueous $NaNO_3$ solution that had been previously illuminated for 3 h (see Figure 6).

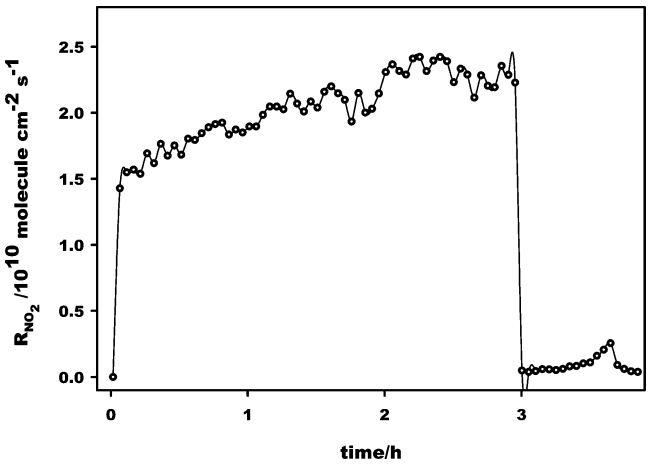

Figure 8. NO_2 emission rates, R_{NO_2}, from a 50 mM aqueous $NaNO_3$ solution illuminated at −30 °C for 3 h, and then warmed at 0.5 °C min^{-1} in the dark for 1 h.

plausibility of this scenario is supported by previous experiments showing that NO_2^- is uniformly produced via reaction 2 down to ∼300 μm in weakly absorbing nitrate-doped ice deposits, whereas NO_2, which is also formed along NO_2^- via reaction 1, is only released from the outermost layers.[10] Secondary NO_2 photolysis, reaction 4, i.e., local NO production, is, therefore, enhanced in deeper layers on account of NO_2 longer residence times, and possibly limited by the increasingly attenuated photon fluxes. Note that NO_2 residence times and light attenuation may have, in principle, different depth profiles.

Also at variance with R_{NO_2}, R_{NO} markedly increases at −20 °C (cf. Figures 1 and 5). From the slope of the log R_{NO} vs 1000/T plot (Figure 3) we obtain an apparent activation energy: E_{NO} = (34.6 ± 6.5) kJ mol^{-1}, which is similar to the E_{NO_2} value derived above. It should be emphasized again that, given the nature of the observed phenomena, these apparent activation energies reflect the interplay of various processes, rather than a single elementary reaction. Some of these processes, such as mass transport through a solid whose morphology undergoes metamorphic transitions, may have non-Arrhenius temperature dependences. Note, however, that E_{NO_2} is about twice as large as E_1, the activation energy for in situ production of •OH radicals, the complementary product of reaction 1, in ice.[9] The ratio $R_{NO_2}/R_{•OH}$ decreases at lower temperatures because the competition between NO_2 escape into the gas phase and chemical and/or photochemical NO_2 losses involves mesoscopic displacements through powder ice, whereas the rates at which •OH radicals escape the solvent cage reflect molecular displacements.[17,37] These arguments point to the inextricable coupling between photochemistry and mass transfer in polycrystalline ice. The coupling is inextricable because the competition between photochemical change and mass transfer is not local, as is the escape of the geminate products of reaction 1 from the solvent cage, but a function of depth and the morphology of the solid matrix.

To further decouple desorption from photogeneration, we carried out experiments in which R_{NO} and R_{NO_2} were measured over a frozen solution subjected to a two-stage schedule consisting of (1) steady illumination at −30 °C for 3 h followed by, (2) heating at 0.5 °C min^{-1} in the dark (Figures 6−9). In stage 1 (Figure 6), R_{NO} is found to slowly build up to a constant value of ∼1.8 × 10^9 molecule cm^{-2} s^{-1} within ∼1 h. Early on in stage 2 (Figures 6 and 7), R_{NO} gradually falls off after illumination has ceased. A broad desorption peak subsequently ensues at ∼−11 °C, consistent with activated desorption/escape from a distribution of occupied sites in a heterogeneous matrix (Figure 7). In contrast, R_{NO_2} rapidly rises up to ∼1.5 × 10^{10} molecule cm^{-2} s^{-1} upon illumination but continues to increase up to R_{NO_2} ∼ 2.4 × 10^{10} molecule cm^{-2} s^{-1} over 3 h (Figure

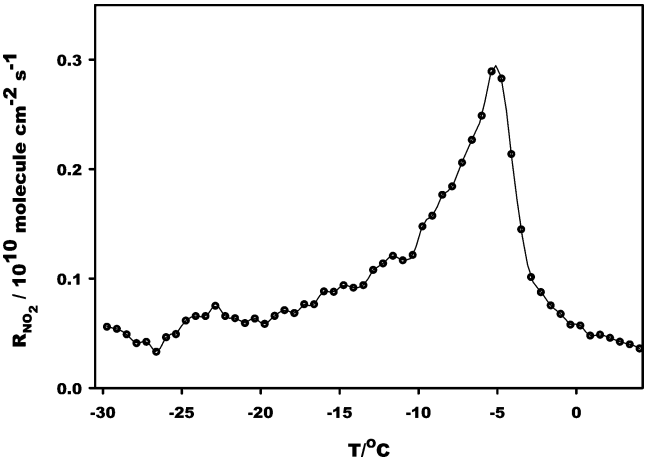

Figure 9. NO_2 emission rates, R_{NO_2}, during a 0.5 °C min^{-1} dark thermogram performed on a frozen 50 mM aqueous $NaNO_3$ solution that had been previously illuminated for 3 h (see Figure 8; cf. Figure 6).

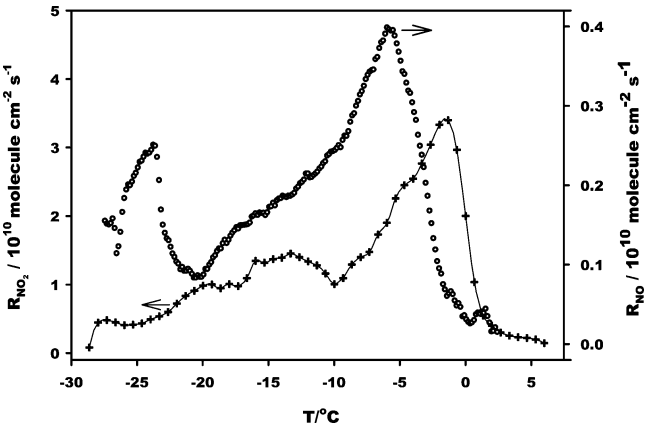

Figure 10. R_{NO} and R_{NO_2} emission rates from a continuously illuminated (at 313 ± 20 nm) 50 mM aqueous $NaNO_3$ solution frozen at −30 °C and warmed to 5 °C at 0.7 °C min^{-1}.

8). R_{NO_2} precipitously drops 70-fold early in stage 2, before bursting at ∼−5 °C (Figure 9). These experiments confirm that NO is more loosely bound than NO_2 to polycrystalline ice.[38] The dissimilar diffusivities of NO and NO_2 may be associated with differences in molecular size and polarity in relation to the microscopic structure of the ice matrix.[39,40]

Another perspective into the complexity of this system is provided by the total amounts of NO, ΣNO, and NO_2, ΣNO_2, liberated in the course of experiments performed by heating frozen 50 mM $NaNO_3$ solutions from −30 to 0 °C at $\mathscr{H}$ = 0.7 and 0.1 °C min^{-1} (Figures 10 and 11) under steady illumination. As we have seen, instantaneous R_{NO} and R_{NO_2} do not represent photochemical production fluxes because, among other reasons, NO and NO_2 might transitorily accumulate in the solid before desorption (eq 6). However, if that were the only reason, all the NO and NO_2 produced by photolysis should be eventually recovered after melting. Therefore, at constant irradiance, because photon dose scales with irradiation time, i.e., with $\mathscr{H}^{-1}$, in the absence of secondary losses, both ΣNO and ΣNO_2 should increase 7-fold from the $\mathscr{H}$ = 0.7 °C min^{-1} thermogram (Figure 10) to that at $\mathscr{H}$ = 0.1 °C min^{-1} (Figure 11). This is clearly not the case: ΣNO increases less than 2-fold, from 5.5 to 9.5, whereas ΣNO_2 only increases by a factor of 3, from 42 to 122 (Σ's in arbitrary units), in these experiments. Thus, the longer photolysis experiment fails to release the expected amounts of NO and NO_2 into the gas-phase, and $\beta = \Sigma NO_2/\Sigma NO$ increases

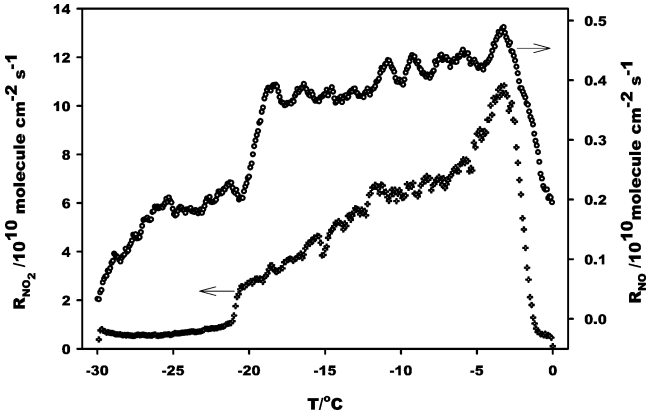

Figure 11. R_{NO} and R_{NO_2} emission rates from a continuously illuminated (at 313 ± 20 nm) 50 mM aqueous $NaNO_3$ solution frozen at −30 °C and warmed to 5 °C at 0.1 °C min^{-1}.

from 7.6 at $\mathscr{H}$ = 0.7 °C min^{-1} to 12.8 at $\mathscr{H}$ = 0.1 °C min^{-1}. The anomaly can be ascribed to the loss of photochemically generated NO_2 via thermal or photochemical reactions prior to desorption. The condition $R_{NO} \ll R_{NO_2}$ rules out secondary photolysis, reaction 4, at the exclusive cause of NO_2 deficits. We have proposed that NO_2 is hydrolyzed back to nitrate and nitrite via a second-order reaction in $[NO_2]$, even at temperatures below the $NaNO_3$ eutectic:[15]

$$2NO_2(g) + H_2O(l) \rightleftarrows NO_3^-(aq) + NO_2^-(aq) + 2H^+(aq) \quad (7)$$

Given these considerations, the fact that ΣNO does not scale with irradiation time may be also a consequence of NO_2 hydrolysis, and the fact that the photolysis of aqueous nitrite is less efficient that the photolysis of gaseous NO_2, i.e., $\varphi_3 \ll \varphi_4$.[24,35] Although reaction 7 is magnified in experiments performed on more concentrated frozen nitrate solutions, we found that NO_2 hydrolysis is still significant in the micromolar range.[15] The reason is that solute concentrations in the microscopic fluid phases in which these reactions actually occur are vastly different from those measured upon melting. The fact that the NO_2 photogenerated in deep ice layers begins to desorb above ∼−5 °C (see above) will only enhance the extent of hydrolytic losses. Figures 10 and 11 dramatically show that time and temperature are linked in these experiments via feedbacks involving gas desorption, secondary thermal/photochemical losses and polycrystalline ice morphology.

Implications for Polar Snowpack Chemistry

Our study shows that product distribution and transport within ice critically affect the observable manifestations of photochemistry. These phenomena will depend on the microscopic and mesoscopic structures of polycrystalline ice. However, there are not canonical ices in nature.[41] If there were, it would be still difficult to reproduce them in the laboratory. Present experimental conditions considerably differ from those prevailing in sunlit snowpacks in a number of ways, such as (1) nitrate concentration ranges (50 mM vs < 20 μM), (2) actinic photon fluxes and spectra, and (3) ice morphology. As a result, absolute NO_x fluxes are about 2 orders of magnitude larger, and the $\gamma = R_{NO}/R_{NO_2}$ ratio up to 10 times smaller than those over snow fields. These considerations underline the fact that field experiments, albeit perhaps more realistic, are site specific. Any generalizations drawn on field experiments require prior identification of the relevant physical and chemical factors. Labora-

tory results, obtained under better controlled conditions, may identify relevant factors, anticipate possible effects, constrain arguments, and eliminate implausible interpretations, but they are not expected to provide quantitative predictions for specific scenarios.

Thus, γ may be larger at lower temperatures because the onset of enhanced ice permeability to NO occurs at lower temperatures than for NO_2. However, it is likely that permeability will depend on ice morphology, i.e., on the mechanism of ice formation. We confirm the prompter release of NO_2 vs NO from nitrate-doped ice upon illumination,[6,42] a phenomenon arising from the fact that NO_2 is a primary photochemical product that only desorbs from external ice layers, whereas NO is a secondary species preferentially formed in deeper ice layers.

It has been pointed out that the consequences of nitrate photolysis in the upper 10 cm of highly porous snow vs water bodies are different because photolysis products are unlikely to escape without further reaction from the latter.[43] Our results show that NO_2 also undergoes hydrolysis before emerging from ice, even below the eutectic. The significant increase of γ with cutoff wavelength over Antarctic snow illuminated with light from a Xenon-arc through long pass filters: $\gamma = 0.55$ (no filter), $\gamma = 0.82$ ($\lambda \geq 295$ nm), and $\gamma = 2.78$ ($\lambda \geq 320$ nm),[3] indirectly supports present low γ values at $\lambda = 313 \pm 20$ nm, confirms that the immediate precursors of NO absorb at wavelengths longer than nitrate itself, and suggests that γ may be a sensitive function of the actinic light spectrum. Any possible role for HONO as a photochemical precursor of NO will be conditional to the local acidity of snow vs $pK_a(HONO) = 2.8$.[30] Work is in progress on the effect of radical scavengers and spectator ionic species, such as those present in natural snow, on nitrate photochemistry.

Acknowledgment. C.S.B. acknowledges support from the Betty and Gordon Moore Foundation. This work was financed by NSF grants ATM-0228140 (Caltech) and ATM-0138669 (Berkeley).

References and Notes

(1) Honrath, R. E.; Peterson, M. C.; Guo, S.; Dibb, J. E.; Shepson, P. B.; Campbell, B. *Geophys. Res. Lett.* **1999**, *26*, 695.

(2) Jones, A. E.; Weller, R.; Wolff, E. W.; Jacobi, H. W. *Geophys. Res. Lett.* **2000**, *27*, 345.

(3) Cotter, E. S. N.; Jones, A. E.; Wolff, E. W.; Bauguitte, S. J. B. *J. Geophys. Res.-Atmos.* **2003**, *108*.

(4) Oncley, S. P.; Buhr, M.; Lenschow, D.; Davis, D.; Semmer, S. R. *Atmos. Environ.* **2004**, *38*, 5389.

(5) Davis, D.; Chen, G.; Buhr, M.; Crawford, J.; Lenschow, D.; Lefer, B.; Shetter, R.; Eisele, F.; Maulding, L.; Hogan, A. *Atmos. Environ.* **2004**, *38*, 5375.

(6) Dibb, J. E.; Arsenault, M.; Peterson, M. C.; Honrath, R. E. *Atmos. Environ.* **2002**, *36*, 2501.

(7) Honrath, R. E.; Guo, S.; Peterson, M. C.; Dziobak, M. P.; Dibb, J. E.; Arsenault, M. A. *J. Geophys. Res.* **2000**, *105*, 24183.

(8) Davis, D.; Nowak, J. B.; Chen, G.; Buhr, M.; Arimoto, R.; Hogan, A.; Eisele, F.; Mauldin, L.; Tanner, D.; Shetter, R.; Lefer, B.; McMurry, P. *Geophys. Res. Lett.* **2001**, *28*, 3625.

(9) Chu, L.; Anastasio, C. *J. Phys. Chem. A* **2003**, *107*, 9594.

(10) Dubowski, Y.; Colussi, A. J.; Hoffmann, M. R. *J. Phys. Chem. A* **2001**, *105*, 4928.

(11) Yang, J.; Honrath, R. E.; Peterson, M. C.; Dibb, J. E.; Sumner, A. L.; Shepson, P. B.; Frey, M.; Jacobi, H. W.; Swanson, A.; Blake, N. *Atmos. Environ.* **2002**, *36*, 2523.

(12) Honrath, R. E.; Lu, Y.; Peterson, M. C.; Dibb, J. E.; Arsenault, M. A.; Cullen, N. J.; Steffen, K. *Atmos. Environ.* **2002**, *36*, 2629.

(13) Dibb, J. E.; Huey, L. G.; Slusher, D. L.; Tanner, D. J. *Atmos. Environ.* **2004**, *38*, 5399.

(14) Beine, H. J.; Domine, F.; Ianniello, A.; Nardino, M.; Allegrini, I.; Teinila, K.; Hillamo, R. *Atmos. Chem. Phys.* **2003**, *3*, 335.

(15) Boxe, C. S.; Colussi, A. J.; Hoffmann, M. R.; Murphy, J.; Wooldridge, P. J.; Betram, T.; Cohen, R. C. *J. Phys. Chem. A.* **2005**, *109*, 8520.

(16) Boxe, C. S.; Colussi, A. J.; Hoffmann, M. R.; Tan, D.; Mastromarino, J.; Case, A. T.; Sandholm, S. T.; Davis, D. D. *J. Phys. Chem. A* **2003**, *107*, 11409.

(17) Dubowski, Y.; Colussi, A. J.; Boxe, C.; Hoffmann, M. R. *J. Phys. Chem. A* **2002**, *106*, 6967.

(18) Calvert, J. G.; Pitts, J. N. *Photochemistry*; Wiley: New York, 1966.

(19) Ridley, B. A.; Walega, J. G.; Dye, J. E.; Grahek, F. E. *J. Geophys. Res.* **1994**, *99*, 25519.

(20) Ridley, B.; Walega, J.; Montzka, D.; Grahek, F.; Atlas, E.; Flocke, F.; Stroud, V.; Deary, J.; Gallant, A.; Boudries, H.; Bottenheim, J.; Anlauf, K.; Worthy, D.; Sumner, A. L.; Splawn, B.; Shepson, P. *J. Atmos. Chem.* **2000**, *36*, 1.

(21) Clough, P. N.; Thrush, B. A. *Trans. Faraday Soc.* **1967**, *63*, 915.

(22) Thornton, J. A.; Wooldridge, P. J.; Cohen, R. C. *Anal. Chem.* **2000**, *72*, 528.

(23) Mack, J.; Bolton, J. R. *J. Photochem. Photobiol. A-Chem.* **1999**, *128*, 1.

(24) Mark, G.; Korth, H. G.; Schuchmann, H. P.; vonSonntag, C. *J. Photochem. Photobiol. A-Chem.* **1996**, *101*, 89.

(25) Daniels, M.; Meyers, R. V.; Belardo, E. V. *J. Phys. Chem.* **1968**, *72*, 389.

(26) Warneck, P.; Wurzinger, C. *J. Phys. Chem.* **1988**, *92*, 6278.

(27) Wagner, I.; Strehlow, H.; Busse, G. *Z. Phys. Chem. Wiesbaden* **1980**, *123*, 1.

(28) Zellner, R.; Exner, M.; Herrmann, H. *J. Atmos. Chem.* **1990**, *10*, 411.

(29) Deister, U.; Warneck, P.; Wurzinger, C. *Ber. Bunsen-Ges. Phys. Chem.* **1990**, *94*, 594.

(30) Riordan, E.; Minogue, N.; Healy, D.; O'Driscoll, P.; Sodeau, J. R. *J. Phys. Chem. A* **2005**, *109*, 779.

(31) Treinin, A.; Hayon, E. *J. Am. Chem. Soc.* **1970**, *92*, 5821.

(32) Zuo, Y. G.; Deng, Y. W. *Chemosphere* **1998**, *36*, 181.

(33) Rotlevi, E.; Treinin, A. *J. Phys. Chem.* **1965**, *69*, 2645.

(34) McEwen, K. L. *J. Chem. Phys.* **1961**, *34*, 547.

(35) DeMore, W. B.; et al. Chemical Kinetics and Photochemical Data for Use in Stratospheric Modeling. Jet Propulsion Laboratory, 1997.

(36) Finlayson-Pitts, B. J.; Pitts, J. N. *Atmospheric Chemistry*; Wiley: New York, 1986.

(37) Kim, J.; Keyes, T. *J. Phys. Chem. B* **2005**, *109*.

(38) Bartels-Rausch, T.; Eichler, B.; Zimmermann, P.; Gaggeler, H. W.; Ammann, M. *Atmos. Chem. Phys.* **2002**, *2*, 235.

(39) Satoh, K.; Uchida, T.; Hondoh, T.; Mae, S. *Proc. NIPR Symp. Polar Metereol. Glaciol.* **1996**, *10*, 73.

(40) Do, J. S.; Wu, K. J.; Tsai, M. L. *Sens. Actuators* **2002**, *B 86*, 98.

(41) Hobbs, P. V. *Ice physics*; Clarendon Press: Oxford, U.K., 1974.

(42) Beine, H. J.; Domine, F.; Simpson, W.; Honrath, R. E.; Sparapani, R.; Zhou, X. L.; King, M. *Atmos. Environ.* **2002**, *36*, 2707.

(43) Wolff, E. W.; Jones, A. E.; Martin, T. J.; Grenfell, T. C. *Geophys. Res. Lett.* **2002**, *29*, 1944.